Volume 2 | Number 10 | October 2018

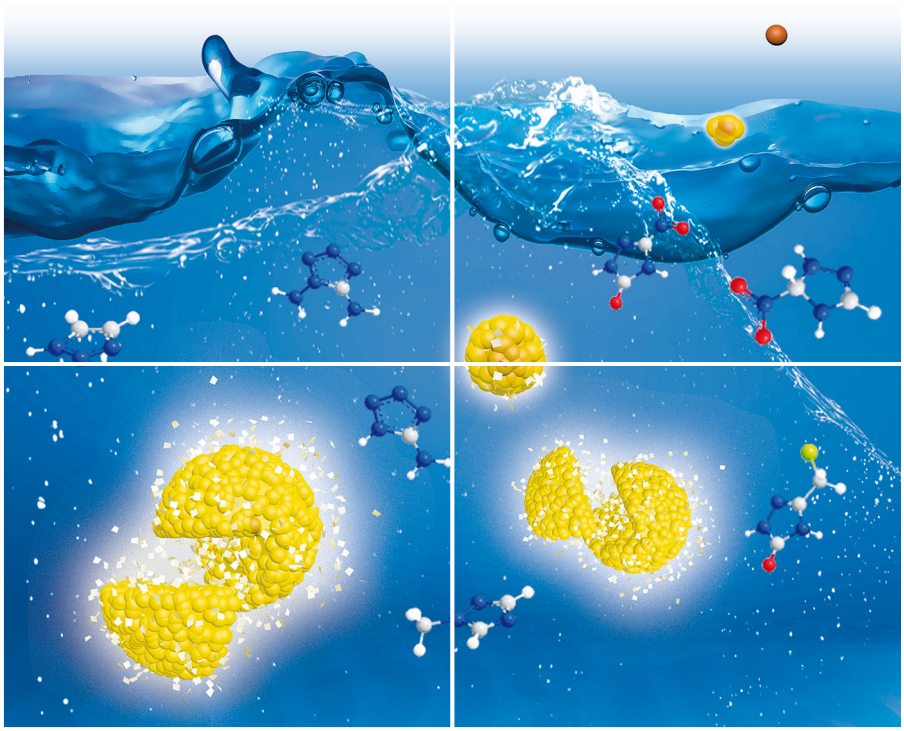

MATERIALS CHEMISTRY

FRONTIERS

Chinese Chemical Society

ROYAL SOCIETY OF CHEMISTRY

rsc.li/frontiers-materials

MATERIALS CHEMISTRY
FRONTIERS

RESEARCH ARTICLE

View Article Online
View Journal | View Issue

Cite this: *Mater. Chem. Front.*, 2018, **2**, 1779

Turn-on fluorescent probe with aggregation-induced emission characteristics for polyazoles†

Yahui Zhang,[a] Weiquan Xu,[a] Lingwei Kong,[a] Bingru Han,[a] Zhengxu Cai, *[a] Jianbing Shi,[a] Bin Tong,[a] Yuping Dong *[a] and Benzhong Tang[b]

Received 15th May 2018,
Accepted 13th June 2018

DOI: 10.1039/c8qm00235e

rsc.li/frontiers-materials

Polyazoles are a class of explosives and the synthetic precursors of antibiotics. The detection of polyazole compounds is quite important but challenging. In this work, a novel fluorescent probe with AIE-activity was designed and synthesized. The probe displays dramatic turn-on behavior and visible distinguishability by the naked eye in the presence of 5-nitro-2,4-dihydro-3*H*-1,2,4-triazole-3-one (NTO) with a limit of detection (LOD) of 7 nM in a water/THF mixture. In addition, the probe shows a high sensitivity to most of the polyazoles, while other common explosives and imidazoles induced a fairly low interference effect, which makes the probe potentially applicable in monitoring water quality.

Polyazoles are aromatic five-membered nitrogen/carbon heterocycles, including triazoles,[1] tetrazoles,[1d,2] and pentazoles.[3,4] Polyazole derivatives have biological and/or pharmaceutical activities and are employed as vital units in antibiotics.[5] For example, triazoles can be used as antifungal, antibacterial, antiviral, analgesic, and antituberculosis agents,[6] while tetrazoles may serve as lipophilic spacers and carboxylic acid surrogates in biologically active molecules.[7] Therefore, both triazoles and tetrazoles widely appear in some well-known antibiotics and are of importance as precursors in synthesis.[8] However, the abuse of these antibiotics has led to a high level of antibiotic residues and they have been noticed as a class of important organic pollutants in water. Various polyazole compounds from antibiotic synthesis or livestock farms have been detected in both surface and ground water, and even in drinking water. Similarly, polyazoles widely used as explosives are another source of organic pollutants in wastewater.[9] Differing from the other nitroaromatic explosives, polyazoles are highly soluble in water, which further raises the risk of water pollution.[10] Therefore, monitoring and detecting polyazoles are quite important not only for biomedical studies but also for environmental conservation.[11] Different analytical techniques that have been applied for trace polyazole sensing include liquid chromatography-mass spectrometry (LC-MS), gas chromatography-mass spectrometry (GC-MS), high-performance liquid chromatography (HPLC), ion mobility spectrometry, proton transfer reaction-mass spectrometry (PTR-MS).[12] However, all of these approaches require expensive instrumentation and/or pre-concentration strategies that render them far less applicable.[13]

Optical sensing is considered as a promising technology for the detection of polyazoles because of its high sensitivity and portability. Aggregation-induced emission (AIE) materials, which fluoresce weakly, or not at all in dilute solutions but are brightly fluorescent when aggregated, offer great opportunities for detection in water.[14] A large number of AIE probes have demonstrated the detection of heavy metal ions,[15] nitroaromatics,[16] and organic pollutants[17] in water. However, the detection of polyazoles in a water system has been rarely reported due to the high affinity binding sites between polyazoles and water molecules. Wang *et al.* reported three AIE-based metal–organic framework (MOF) materials that exhibited high sensitivity toward the triazole explosives.[18] A major concern with the MOF approach is that these chemicals are highly poisonous and are not biodegradable, which limits their usage in the field of environmental protection.[19] Development of environmentally robust, reliable, and inexpensive methods for the detection of polyazoles has been a matter of great concern.

Recently, our group reported a series of novel hexaphenyl-1,3-butadiene (HPB)-based AIEgens (luminogens with AIE) with high emission in their aggregated states. This series of molecules showed highly sensitive mechanochromic, thermalchromic, and photochromic[20] performances. The HPB-based probe was also used to efficiently differentiate structurally similar volatile amines.[21] In this work, we report a novel fluorescent probe for the detection of polyazoles. ***E,E*-HPB-ID** (Scheme 1) with a typical AIE feature shows a visible emission and high quantum

[a] *Beijing Key Laboratory of Construction Tailorable Advanced Functional Materials and Green Applications, School of Materials Science and Engineering, Beijing Institute of Technology, Beijing 100081, China. E-mail: caizx@bit.edu.cn, chdongyp@bit.edu.cn*

[b] *Department of Chemistry, Hong Kong Branch of Chinese National Engineering Research Center for Tissue Restoration and Reconstruction, The Hong Kong University of Science and Technology, Clear Water Bay, Kowloon, Hong Kong, China*

† Electronic supplementary information (ESI) available: Synthetic materials and instruments, synthetic methods, NMR, MS, TEM and SEM. See DOI: 10.1039/c8qm00235e

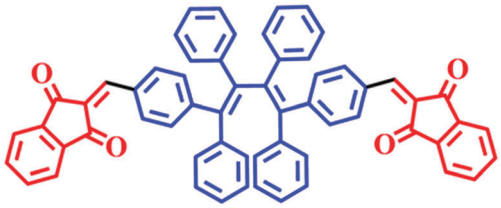

Scheme 1 Molecular structure of ***E,E*-HPB-ID**.

yield (QY) in the solid state (Φ_F = 27.90%). The probe could be self-assembled into various sizes of nanoparticles by carefully tuning the stirrer rotational speeds. Inspired by their emissive characteristics in the aggregated states, ***E,E*-HPB-ID** nanoparticles with a suitable size are applied in the detection of triazoles and tetrazoles in water. The probes displayed a broad spectrum of fluorescence turn-on response toward most of triazoles and tetrazoles. The detection limit of 5-nitro-2,4-dihydro-3*H*-1,2,4-triazole-3-one (NTO) could reach up to 0.9 μg mL^{-1} (7×10^{-6} mol L^{-1}) in water. The results indicated that ***E,E*-HPB-ID** is a favorable material for the detection of polyazoles in water, being potentially useful in monitoring water quality and in biological/biomedical studies.

In order to enable the visible detection of polyazoles, the donor–acceptor (D–A) approach was used to build the probe molecule, in which six phenyl units and two indandiones were employed as the donor and acceptor units, respectively. The molecular structure and synthetic routes of ***E,E*-HPB-ID** are depicted in Scheme 1 and Fig. S1 (ESI†), respectively. Density functional theory (DFT) calculations were used to investigate the molecular conformation and electronic structure of ***E,E*-HPB-ID** (Fig. S5, ESI†). The molecule was found to be twisted because of the strong steric hindrance among the six phenyl rings, which was beneficial for constructing AIE fluorophores and achieving highly bright AIE nanoparticles.

The AIE features of ***E,E*-HPB-ID** were investigated *via* photoluminescence (PL) spectra in THF/water mixtures with different water fractions (f_w) as shown in Fig. 1. The fluorescence intensity of THF/water mixtures with f_w lower than 70% was negligibly small due to the non-radiative decay caused by the free intramolecular rotation of the σ bonds between the phenyl and alkenyl groups. The emission began to increase once f_w reached 70%. The fluorescence intensity of the 90% water fraction increased by ~6 fold. The ultraviolet-visible (UV-Vis) spectra (Fig. S6, ESI†) confirmed the formation of aggregates. Dynamic light scattering (DLS) results showed that the size of the ***E,E*-HPB-ID** aggregates in the 90% water fraction was 79.3 nm (inset of Fig. S6, ESI†). ***E,E*-HPB-ID** was weakly emissive in THF solution with a quantum yield Φ_F = 0.56%, but highly emissive in the THF/water mixture (f_w = 90%) and in the solid powder with Φ_F = 14.84% and Φ_F = 27.90%, respectively, also indicating the AIE feature.

As a proof-of-concept experiment, NTO was selected as the target triazole material (Fig. 2). ***E,E*-HPB-ID** (1×10^{-4} mol L^{-1})[22] was pre-assembled into nanoscale particles with a size of 172 nm in a 90% water fraction solution without stirring rotation.

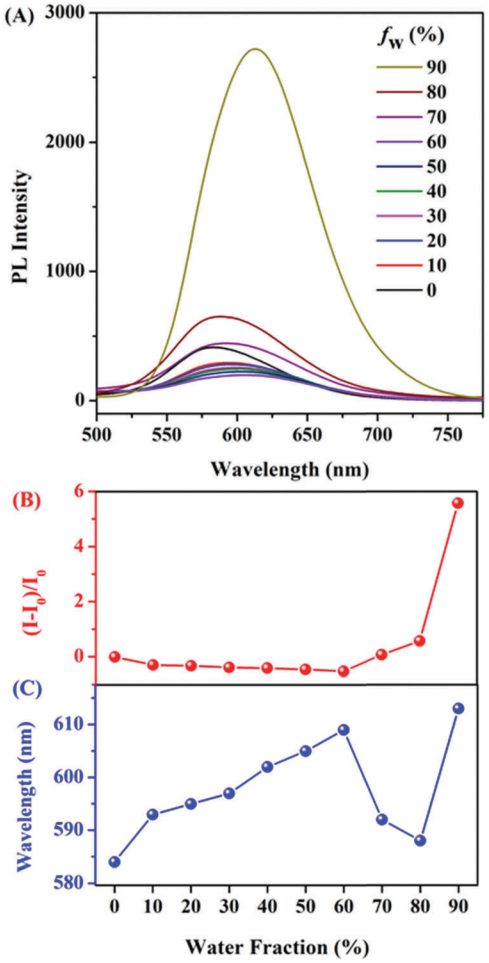

Fig. 1 (A) Photoluminescence (PL) spectra of ***E,E*-HPB-ID** in THF/water mixtures. (B) Correlation between the net change in PL intensity [$(I - I_0)/I_0$], and (C) the wavelength of ***E,E*-HPB-ID** with different water fractions in the THF/water mixtures. [***E,E*-HPB-ID**] = 1×10^{-5} mol L^{-1}; excitation wavelength: 410 nm.

This aggregate was stable and did not coagulate for at least one night (Fig. 2B insets). Upon the titration of freshly prepared nanoparticles with NTO, the PL intensity of the ***E,E*-HPB-ID** particles enhanced up to 3-fold (black line in Fig. 2B). The dissociated ***E,E*-HPB-ID** nanoparticles further aggregated to a larger formation (~2100 nm determined by DLS), and the emission boosted as a result of the restriction of intramolecular rotations. The maximum emission wavelengths gradually blue-shift (20 nm) as well, most likely because the condensed packing further twisted the molecular conformations.

It's worth mentioning that the nanoparticle size could be systematically tuned by varying the stirrer rotational speeds during the incubation process, while the response sensitivity to NTO was associated with the different sizes of aggregates. The fluorescent turn-on efficiency can be quantitatively explained by the Stern–Volmer equation in Table 1. As shown in Fig. 2A, the sizes of the aggregates decreased with increasing revolutions. Stirring at a rate of 1000 revolutions per minute (rpm) decreased the size of the aggregates from 172 nm (no stirring rotation) to

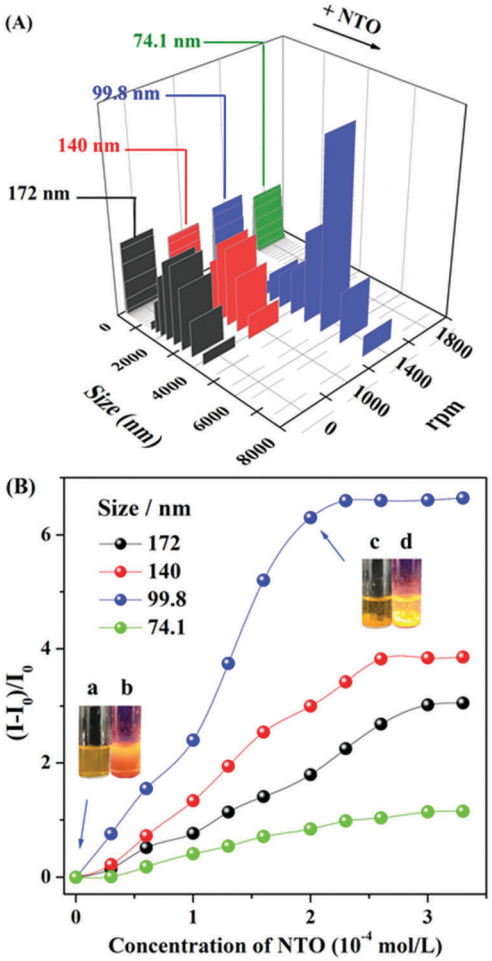

Fig. 2 (A) Dynamic light scattering (DLS) results of ***E,E*-HPB-ID** *versus* different stirring rotational speeds in 90% water fraction before and after the addition of NTO (2 eq.); (B) Stern–Volmer plots of different sizes of ***E,E*-HPB-ID** aggregates in 90% water fraction upon incremental addition of NTO. Inset picture, (a and b): 90% water fraction without NTO under sunlight and UV light; (c and d): 90% water fraction with NTO (2 eq.) under sunlight and UV light at a size of 99.8 nm. Stern–Volmer equation: $(I_0/I) = 1 + K_{sv}[Q]$, where K_{sv} is the quenching constant (M^{-1}), [Q] is the molar concentration of the analyte, and I_0 and I are the luminescence intensities before and after the addition of the analyte, respectively. [***E,E*-HPB-ID**] = 1×10^{-4} mol L^{-1}; excitation wavelength: 410 nm.

Table 1 Values of the quenching constants (K) for NTO

Particle sizes/nm	172	140	99.8	74.1
K_{sv}/M^{-1}	610	770	1330	230

140 nm. These smaller sizes of aggregates showed a higher sensitivity to NTO with a K_{sv} value (Table 1) of 770 M^{-1} and ~3.9 folds enhancement in the presence of 2 equiv. of NTO. The probe with a particle size of 99.8 nm has the highest K_{sv} value of 1330 M^{-1} toward NTO along with ~6.7 fold fluorescence enhancement (Fig. 2B and Fig. S7, ESI†). The DLS results demonstrated that the particle size increased from 99.8 nm to ~5000 nm with the addition of 2 equiv. of NTO. Luminescent sediments could be observed directly by the naked eye (inset pictures of Fig. 2B). Minor change occurred after the addition of NTO when the particle size was further decreased to 74 nm (Fig. S8, ESI†). Based on the K_{sv} values and the standard deviations for three repeated fluorescent measurements of blank solutions, the limit of detection (LOD) of ***E,E*-HPB-ID** with a size of 99.5 nm toward NTO was calculated to be 0.9 μg mL^{-1} (7×10^{-6} mol L^{-1}).

The universal detection of polyazoles in water systems is highly desirable for practical applications in the detection of antibiotic residues and wastewater monitoring. To explore the sensitivity of ***E,E*-HPB-ID** to other polyazoles, fluorescence titrations were carried out with incremental addition of several triazoles and tetrazoles to water where ***E,E*-HPB-ID** was dispersed. Six more triazoles and tetrazoles, five classes of common explosives and three imidazole derivatives were checked (Fig. 3, Table S1 and Fig. S9, ESI†). All measurements were performed 270 s after the addition of each target compound to ensure that a steady intensity of fluorescence had been achieved. As compared to common explosives (PA, TNT, HMX, CL-20 and RDX) and imidazole derivatives (N-IM, 2N-IM and IM), triazole and tetrazole derivatives demonstrated an outstanding "turn-on" response as shown in Fig. 3, suggesting that most of the explosives did not interfere with the detection of polyazoles in water (Table S2, ESI†). In addition, ***E,E*-HPB-ID** displays only a very weak turn-on behavior to RDX, while its fluorescence was quenched in the presence of other nitroaromatic compounds, indicating that the probe is potentially applicable to distinguish polyazole explosives and nitroaromatic explosives.

To better understand the turn-on response of ***E,E*-HPB-ID** toward NTO, NMR titration, scanning electron microscopy (SEM) and transmission electron microscopy (TEM) were performed. ^{1}H NMR images of ***E,E*-HPB-ID** in THF-d_8 and NTO in H_2O with different molar ratios is shown in Fig. S10 (ESI†) (volume of THF-d_8 and H_2O remained constant). With the incremental addition of NTO, no other signal changed except for the signal enhancement of the NTO peaks, indicating that no reaction occurred during the titration process. In addition, the UV-vis absorption spectra were the sum of the corresponding components after the addition of NTO (Fig. S11, ESI†). Fig. 4 shows the SEM images of the nanoaggregates in as-prepared samples of ***E,E*-HPB-ID**, NTO and their mixtures, respectively. ***E,E*-HPB-ID** exhibited a spherical morphology (Fig. 4A), while NTO exhibited a sheet-like morphology (Fig. 4D). Some rods emerged among the spheres after the addition of NTO (Fig. 4G, Fig. S13, ESI†), indicating that NTO could induce crystallization of ***E,E*-HPB-ID** aggregates. In addition, the size of the aggregates of ***E,E*-HPB-ID** (determined by SEM, in Fig. S12C, ESI†) increased to 5 μm upon the addition of NTO, which was consistent with the DLS results.

The formation of crystallized ***E,E*-HPB-ID** and NTO aggregates was further evident by the TEM (Fig. 4B, E and H) and selected-area electron diffraction (SAED) patterns. The SAED patterns of the ***E,E*-HPB-ID** + NTO nanoparticles showed diffraction features with a d-value of 3.15 Å, while ***E,E*-HPB-ID** and NTO showed ring like patterns with an amorphous morphology. The d-value of the ***E,E*-HPB-ID** + NTO mixture was larger than those of either ***E,E*-HPB-ID** or NTO suggesting

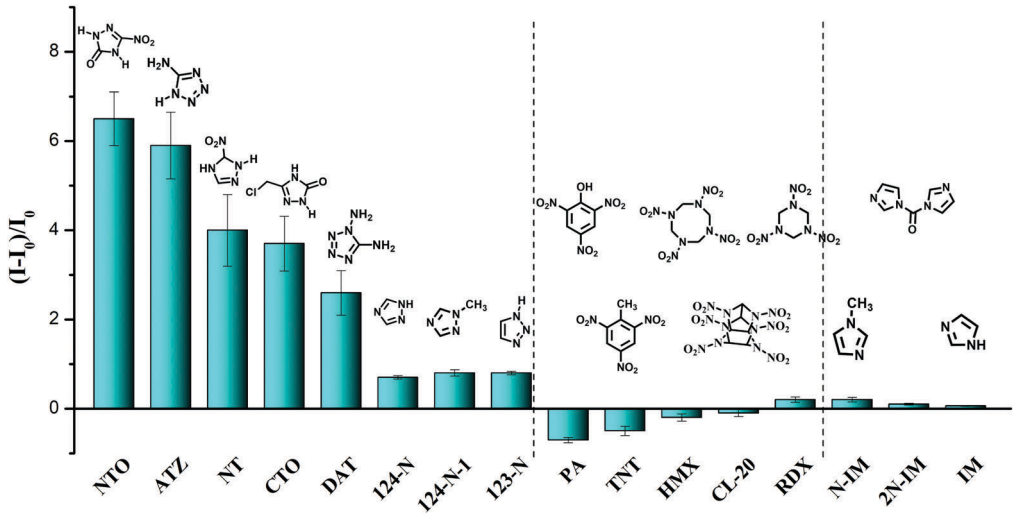

Fig. 3 Fluorescence enhancement ($(I - I_0)/I_0$) of ***E,E*-HPB-ID** by different analytes ($M_{\textbf{\textit{E,E}-HPB-ID}} : M_{analytes} = 1:2$) in the 90% water fraction in THF/water mixtures. [***E,E*-HPB-ID**] = 1×10^{-4} mol L^{-1}.

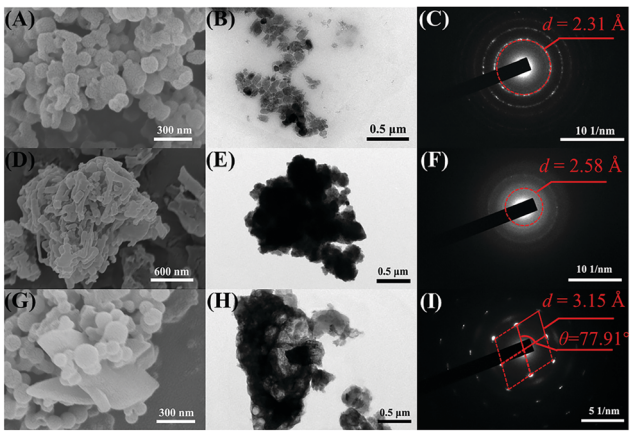

Fig. 4 SEM images of (A) ***E,E*-HPB-ID**, (D) NTO and (G) ***E,E*-HPB-ID** + NTO; TEM images of (B) ***E,E*-HPB-ID**, (E) NTO and (H) ***E,E*-HPB-ID** + NTO; SAED patterns of (C) ***E,E*-HPB-ID**, (F) NTO and (I) ***E,E*-HPB-ID** + NTO.

that NTO not only induced ***E,E*-HPB-ID** nanoparticles to further aggregate, but also penetrated into the lattices of ***E,E*-HPB-ID** nanoparticles. In addition, as compared to the pattern of ***E,E*-HPB-ID**, higher order diffraction spots were observed in the mixture patterns (Fig. 4I), indicating that along with NTO, the degree of crystallization of ***E,E*-HPB-ID** gradually increased, resulting in the restriction of intramolecular rotations. Therefore, the suitable size of ***E,E*-HPB-ID** nanoparticles was more sensitive to NTO, because NTO can penetrate into ***E,E*-HPB-ID** nanoparticles. The close packing and high crystalline structure resulted in a turn-on response to the NTO series compounds.

Conclusions

In conclusion, a new probe with a typical AIE property was developed for the detection of polyazoles. The ***E,E*-HPB-ID** probe showed a high sensitivity to a broad spectrum of triazoles and tretrazoles, such as NTO, ATZ, NT, CTO and DAT. The detection was visible to the naked eye with a ~6.65 fold fluorescence enhancement under optimal conditions. This enhancement was attributed to the aggregation of the ***E,E*-HPB-ID** probe induced by NTO. Although the mechanism of the intermolecular interaction between the probe and polyazoles is not very clear, the method showed advantages of universality, high sensitivity, and ease of visualization and can be practically used for the detection of polyazoles in wastewater.

Conflicts of interest

There are no conflicts to declare.

Acknowledgements

This work was financially supported by the National Natural Scientific Foundation of China (Grant No. 51673024, 21474009, 51328302), the National Basic Research Program of China (973 Program; Grant No. 2013CB834704), the Beijing Institute of Technology Research Fund Program for Young Scholars and the Graduate Technological Innovation Project of Beijing Institute of Technology.

Notes and references

1 (*a*) B. Schulze and U. S. Schubert, *Chem. Soc. Rev.*, 2014, **43**, 2522–2571; (*b*) C. W. Tornøe, C. Christensen and M. J. Meldal, *Org. Chem.*, 2002, **67**, 3057–3064; (*c*) G. Aromí, L. A. Barrios, O. Roubeau and P. Game, *Coord. Chem. Rev.*, 2011, **255**, 485–546.

2 (*a*) H. Zhao, Z. R. Qu, Y. H. Ye and R. G. Xiong, *Chem. Soc. Rev.*, 2008, **37**, 84–100; (*b*) N. Szimhardt, M. H. H. Wurzenberger, A. Beringer, L. J. Daumann and J. Stierstorfer, *J. Mater. Chem. A*, 2017, **5**, 23753–23765.

3 (*a*) Y. Z. Yang, X. F. Liu, R. B. Zhang and S. P. Pang, *Phys. Chem. Chem. Phys.*, 2017, **19**, 31236–31244; (*b*) Y. G. Xu, Q. Wang, C. Shen, Q. H. Lin, P. C. Wang and M. Lu, *Nature*, 2017, **549**, 78–81; (*c*) K. F. Ferrist and R. J. Bartlett, *J. Am. Chem. Soc.*, 1992, **114**, 8302–8303; (*d*) J. J. Dong, K. Wang., M. Wang, P. Yu and L. Q. Mao, *J. Am. Chem. Soc.*, 2017, **139**, 5877–5882.

4 Pentazole, as a highly energetic material, is only stable in the state of an anionic salt and is excluded in the following discussion.

5 R. D. Santo, *Nat. Prod. Rep.*, 2010, **27**, 1084–1098.

6 (*a*) W. S. Horne, M. K. Yadav, C. D. Stout and M. R. Ghadiri, *J. Am. Chem. Soc.*, 2004, **126**, 15366–15367; (*b*) A. D. Moorhouse, A. M. Santos, M. Gunaratnam, M. Moore, S. Neidle and J. E. Moses, *J. Am. Chem. Soc.*, 2006, **128**, 15972–15973.

7 K. Cheng, J. S. Lee, P. L. Hao, S. Q. Yao, K. Ding and Z. Q. Li, *Angew. Chem., Int. Ed.*, 2017, **56**, 15044–15048.

8 M. Nishino, K. Hirano, T. Satoh and M. Miura, *Angew. Chem., Int. Ed.*, 2013, **52**, 4457–4461.

9 (*a*) B. Wang, X. L. Lv, D. W. Feng, L. H. Xie, J. Zhang, M. Li, Y. B. Xie, J. R. Li and H. C. Zhou, *J. Am. Chem. Soc.*, 2016, **138**, 6204–6216; (*b*) C. M. Santana, Z. S. Ferrera, M. E. T. Padrón and J. J. S. Rodríguez, *Molecules*, 2009, **14**, 298–320.

10 (*a*) W. R. Liu, Y. Y. Yang, Y. S. Liu, L. J. Zhang, J. L. Zhao, Q. Q. Zhang, M. Zhang, J. N. Zhang, Y. X. Jiang and G. G. Ying, *J. Hazard. Mater.*, 2017, **329**, 310–320; (*b*) C. H. Lin, P. H. Chou and P. J. Chen, *J. Hazard. Mater.*, 2014, **277**, 150–158.

11 R. S. Shapiro, N. Robbins and L. E. Cowen, *Microbiol. Mol. Biol. Rev.*, 2011, **75**, 213–267.

12 J. Rosenthal and S. J. Lippard, *J. Am. Chem. Soc.*, 2010, **132**, 5536–5537.

13 B. Nadia, S. Khaled and B. Nasser, *Clin. Microbiol. Rev.*, 2017, **30**, 4.

14 (*a*) J. D. Luo, Z. L. Xie, J. W. Y. Lam, L. Cheng, H. Y. Chen, C. F. Qiu, H. S. Kwok, X. W. Zhan, Y. Q. Liu, D. B. Zhu and B. Z. Tang, *Chem. Commun.*, 2001, 1740–1741; (*b*) R. R. Hu, N. L. C. Leungb and B. Z. Tang, *Chem. Soc. Rev.*, 2014, **43**, 4494–4562; (*c*) J. Mei, N. L. C. Leung, R. T. K. Kwok, J. W. Y. Lam and B. Z. Tang, *Chem. Rev.*, 2015, **115**, 11718–11940; (*d*) Y. Wu, A. J. Qin and B. Z. Tang, *Chin. J. Polym. Sci.*, 2017, **35**, 141–154; (*e*) J. G. Wang, X. G. Gu, P. F. Zhang, X. B. Huang, X. Y. Zheng, M. Chen, H. T. Feng, R. T. K. Kwok, J. W. Y. Lam and B. Z. Tang, *J. Am. Chem. Soc.*, 2017, **139**, 16974–16979; (*f*) Y. Z. Chen, X. M. Shi, Z. L. Lu, X. F. Wang and Z. Wang, *Anal. Chem.*, 2017, **89**, 5278–5284.

15 (*a*) T. Y. Han, X. Feng, B. Tong, J. B. Shi, L. Chen, J. G. Zhi and Y. P. Dong, *Chem. Commun.*, 2012, **48**, 416–418; (*b*) Y. N. Hong, S. J. Chen, C. W. T. Leung, J. W. Y. Lam, J. Z. Liu, N. W. Tseng, R. T. K. Kwok, Y. Yu, Z. K. Wang and B. Z. Tang, *ACS Appl. Mater. Interfaces*, 2011, **3**, 3411–3418; (*c*) G. Kumar, K. Paul and V. Luxami, *Sens. Actuators, B*, 2018, **263**, 585–593; (*d*) M. Shyamal, S. Maity, A. Maity, R. Maity, S. Roy and A. Misra, *Sens. Actuators, B*, 2018, **268**, 347–359.

16 (*a*) X. Z. Yan, H. Wang, C. E. Hauke, T. R. Cook, M. Wang, M. L. Saha, Z. X. Zhou, M. M. Zhang, X. P. Li, F. H. Huang and P. Stang, *J. Am. Chem. Soc.*, 2015, **137**, 15276; (*b*) W. Huang, M. Bender, K. Seehafer, L. Wacker, R. R. Schröder and U. H. F. Bunz, *Macromolecules*, 2018, **51**, 1345–1350; (*c*) Q. Y. Li, Z. Ma, Z. Li, W. Q. Zhang, J. L. Xu, W. Wei, H. Lu, X. S. Zhao and X. J. Wang, *Chem. Commun.*, 2016, **52**, 11284–11287; (*d*) W. L. Che, G. F. Li, X. M. Liu, K. Z. Shao, D. X. Zhu, Z. M. Su and M. R. Bryce, *Chem. Commun.*, 2018, **54**, 1730–1733.

17 J. S. Wu, W. M. Liu, J. C. Ge, H. Y. Zhang and P. F. Wang, *Chem. Soc. Rev.*, 2011, **40**, 3483–3495.

18 Y. X. Guo, X. Feng, T. Y. Han, S. Wang, Z. G. Lin, Y. P. Dong and B. Wang, *J. Am. Chem. Soc.*, 2014, **136**, 15485–15488.

19 (*a*) M. Eddaoudi, J. Kim, N. Rosi, D. Vodak, J. Wachter, M. O'Keeffe and O. M. Yaghi, *Science*, 2002, **295**, 469–472; (*b*) H. Furukawa, K. E. Cordova, M. O'Keeffe and O. M. Yaghi, *Science*, 2013, **341**, 1230444; (*c*) J. Li, X. X. Wang, J. X. Zhao, C. L. Chen, Z. F. Chai, A. Alsaedi, T. Hayat and X. K. Wang, *Chem. Soc. Rev.*, 2018, **47**, 2322–2356.

20 (*a*) Y. H. Zhang, L. W. Kong, X. L. Pan, H. L. Mao, X. K. Zeng, J. B. Shi, B. Tong and Y. P. Dong, *Dyes Pigm.*, 2017, **139**, 714–719; (*b*) Y. H. Zhang, L. W. Kong, H. L. Mao, X. L. Pan, J. B. Shi, B. Tong and Y. P. Dong, *Mater. Chem. Front.*, 2017, **1**, 2569–2573.

21 L. W. Kong, Y. H. Zhang, H. L. Mao, X. L. Pan, Y. Tian, Z. L. Tian, X. K. Zeng, J. B. Shi, B. Tong and Y. P. Dong, *Faraday Discuss.*, 2017, **196**, 101–111.

22 The size of ***E,E*-HPB-ID** aggregates at the concentration of 1×10^{-5} mol L^{-1} was too small (79.3 nm) to respond to polyazoles.